

Sersiclets – A Matched Filter Extension of Shapelets for Weak Lensing Studies

W. Ngan¹, L. Van Waerbeke¹, A. Mahdavi², C. Heymans^{3,1}, H. Hoekstra^{2,4}

¹ University of British Columbia, 6224 Agricultural Road, Vancouver, BC, Canada V6T 1Z1

² Department of Physics and Astronomy, University of Victoria, Victoria, BC, Canada V8P 5C2

³ SUPA, Institute for Astronomy, University of Edinburgh, Blackford Hill, Edinburgh, United Kingdom EH9 3HJ

⁴ Alfred P. Sloan Fellow

30 October 2018

ABSTRACT

The precision study of dark matter using weak lensing by large scale structure is strongly constrained by the accuracy with which one can measure galaxy shapes. Several methods have been devised but none have demonstrated the ability to reach the level of precision required by future weak lensing surveys. In this paper we explore new avenues to the existing *Shapelets* approach, combining a priori knowledge of the galaxy profile with the power of orthogonal basis function decomposition. This paper discusses the new issues raised by this matched filter approach and proposes promising alternatives to shape measurement techniques. In particular it appears that the use of a matched filter (e.g. Sérsic profile) restricted to elliptical radial fitting functions resolves several well known Shapelet issues.

Key words: Cosmology – dark matter: gravitational lensing.

1 INTRODUCTION

Galaxy shapes provide the unique signature of gravitational lensing by large scale structure, which has been recognized as a key to the study of dark matter and dark energy (Munshi et al. 2008). A limiting factor is the accuracy with which one can measure shapes (Heymans et al. 2006; Massey et al. 2007; Hoekstra & Jain 2008). Among the different existing methods, one particularly interesting approach is the decomposition of galaxy images using basis functions e.g. Bernstein & Jarvis (2002) or *Shapelets* (Refregier 2003; Refregier & Bacon 2003; Massey & Refregier 2005). The strengths of this approach rely on the fact that the shape measurement is analytical and therefore time efficient as it involves rather small matrix multiplications. *Shapelets* decompose an image into a linear combination of orthonormal components up to some truncation order, and the shape parameters are extracted from a least-squares best fit using the recomposed (noise free) model. However, the Shapelet type approach suffers from a few difficulties:

(i) The choice of the decomposition truncation order is arbitrary. In practice, different lensing groups use radically different “optimal” truncation orders. Some prefer low (Kuijken 2006), while others prefer high (Bergé et al. 2008), although the χ^2 values for different truncation order could be very different. Therefore a constant χ^2 criterion to mea-

sure the shape does not appear to be a robust guarantee of unbiased shape measurement.

(ii) “Easy cases” such as large and bright elliptical galaxies are poorly fitted. This suggests that a good fit for low signal-to-noise galaxies does not necessarily mean that the shape has been correctly measured, since it could just be buried in the sky noise. This is the overfitting problem.

(iii) Basis decomposition has too many degrees of freedom for shear measurement, since ideally we are only interested in two numbers (or six if we include the flexion). This is where galaxy morphology and shear measurement are clearly two different problems.

All of those problems have one common origin, namely the choice of the zeroth order weight function – Gaussian functions for both Cartesian (Refregier 2003) and Polar Shapelets (Massey & Refregier 2005), as well as Bernstein & Jarvis (2002). Unfortunately, Gaussian functions are poor matches to real galaxy profiles. Ideally, we would like the zeroth order to be as close as possible to the real profile, and leave to the basis decomposition the task to fit departures from this “typical” profile.

Currently the most promising shape measurement method uses a bayesian model fitting approach (Miller et al. 2007; Kitching et al. 2008). This method does not suffer from the same issues as Shapelets, but is limited by the strong galaxy profile prior.

In this paper, we investigate how the change of the

weight function affects the basis decomposition method, and how it leads naturally to a hybrid method which combines Shapelets and fitting techniques. We choose to focus on the Sérsic profile (hence the term Sersiclets), but our discussion can be extended to any profile¹, e.g. Moffat profile for ground based point spread function (PSF). Section 2 introduces the notation and gives a technical description of the new fitting functions. Section 3 shows the impact of those fitting functions on shape fitting and decomposition. Finally, Section 4 summarizes our work so far and future possibilities.

Note that in this paper we choose not to discuss the PSF deconvolution. Indeed, the problems we mentioned earlier affect equally the measurement of galaxy shapes whether or not the galaxies are convolved with a PSF, and Shapelets are a popular approach because their Gaussian properties allow for very efficient PSF treatment. The PSF deconvolution issue goes beyond this work because it depends on how the PSF is measured and interpolated between stars. Moreover the approach developed here could as well be applied to the PSF profile measurement separately, and then used later to address the deconvolution step through a forward convolution model fitting method. See for example Kitching et al. (2008).

2 METHODOLOGY

2.1 Basis functions in polar coordinates

In 1D, all polynomials $P_k(x)$ of degree k are orthonormal with respect to a weight function $w(x)$ if they satisfy

$$\int_a^b P_i(x)P_j(x)w(x)dx = \delta_{ij}. \quad (1)$$

A particular choice of weight function $w(x)$ uniquely determines the family of polynomials (e.g. for the Cartesian Shapelets, a Gaussian weight defines the Hermite polynomials). A complete set of polynomials can be useful for decomposing an arbitrary function $f(x)$ as a linear combination of *basis functions* $\chi_n(x) = P_n(x)[w(x)]^{1/2}$ such that

$$f(x) = \sum_{n=0}^{\infty} A_n \chi_n(x). \quad (2)$$

In 2D, the basis functions can be represented using polar coordinates. Following the intuition for Polar Shapelets, we separate our basis functions $\chi_{mn}(r, \phi)$ into the radial component $R_n(r)$ and the angular component $e^{im\phi}$. We also assume that the weight function $w(r)$ has no angular dependence. The 2D basis functions $\chi_{mn}(r, \phi)$ in polar coordinates would be in the form

$$\chi_{mn}(r, \phi) = R_n(r)[w(r)]^{1/2} e^{im\phi}. \quad (3)$$

The orthonormality is then written as

$$\int_0^a r dr \int_0^{2\pi} d\phi \chi_{mn}^*(r, \phi) \chi_{m'n'}(r, \phi) = \delta_{mm'} \delta_{nn'} \quad (4)$$

¹ While working on the concepts discussed in this paper, we became aware of similar investigations using exponential and hyperbolic sech functions (Kuijken & van Uitert in prep).

where $*$ denotes complex conjugate. The orthonormality requirements for radial and angular parts, $\int_0^a R_n R_{n'} w(r) r dr = \delta_{nn'}$ and $\int_0^{2\pi} e^{i(m'-m)\phi} d\phi = 2\pi \delta_{mm'}$, can be satisfied independently. In particular, $R_n(r)$ is an orthonormal polynomial of degree n with respect to the weight function $w(r)$. The integration limit a for the radial component will be discussed in Section 2.4.

With an orthogonal and complete set of basis functions, an arbitrary image $f(r, \phi)$ can then be decomposed into

$$f(r, \phi) \approx \sum_{n=0}^{n_{\max}} \sum_{m=-n}^n A_{mn} \chi_{mn}(r, \phi) \quad (5)$$

where the complex basis coefficients A_{mn} satisfy $A_{mn}^* = A_{-m,-n}$ so that $f(r, \phi)$ is wholly real. We will refer n_{\max} as “order” in the following sections.

Readers familiar with Polar Shapelets may notice that our radial component here only requires n , and m increases in steps of 1. In Polar Shapelets, the radial component requires both m and n , and m increases in steps of 2. Our choice to completely decouple the radial and the angular components is of mere convenience, which comes with the cost that our set of “basis functions” is no longer complete. Consequently, our set of *fitting functions* cannot decompose an arbitrary image. As we shall see in Section 2.5 and Section 2.6, though, the lack of completeness is not a hindrance to decomposing images of galaxies for weak lensing, as galaxies follow Sérsic profiles (Sérsic 1968) and are not arbitrary in general.

2.2 Weight function

The basis functions in Shapelets often require high order polynomials to describe galaxy shapes accurately because galaxies’ radial light profiles do not match the weight functions. Galaxies’ light profiles are well described by Sérsic’s empirical formula (Peng et al. 2002):

$$I(r) = I(k) \exp[-b_\lambda (r/k)^{1/\lambda} + b_\lambda] \quad (6)$$

where k is a scale radius, and λ is known as the Sérsic index. For $0.5 \lesssim \lambda \lesssim 10$, $b_\lambda = 2\lambda - 1/3$. We use a parameterized form of Equation 6 as our weight function:

$$w(r) \equiv \exp \left[-(2\lambda - 1/3) \left(\frac{r}{k} \right)^{1/\lambda} \right]. \quad (7)$$

2.3 Radial component

The radial component involves a non-trivial computational step, as $R_n(r)$ must satisfy the orthonormality requirement described in Section 2.1. We obtain $R_n(r)$ by the Gram-Schmidt process². Using Dirac notation $\langle R_i | R_j \rangle \equiv \int R_i(r) R_j(r) w(r) r dr$, the Gram-Schmidt process generates each $R_n(r)$ by a recurrence relation:

$$R_n(r) = \left(r - \frac{\langle r R_{n-1} | R_{n-1} \rangle}{\langle R_{n-1} | R_{n-1} \rangle} \right) R_{n-1} - \frac{\langle R_{n-1} | R_{n-1} \rangle}{\langle R_{n-2} | R_{n-2} \rangle} R_{n-2}$$

where $R_0(r) \equiv 1$, and $R_1(r) = \left(r - \frac{\langle r R_0 | R_0 \rangle}{\langle R_0 | R_0 \rangle} \right) R_0$. After the recurrence step, each $R_n(r)$ is individually normalized.

² <http://mathworld.wolfram.com/Gram-SchmidtOrthonormalization.html>

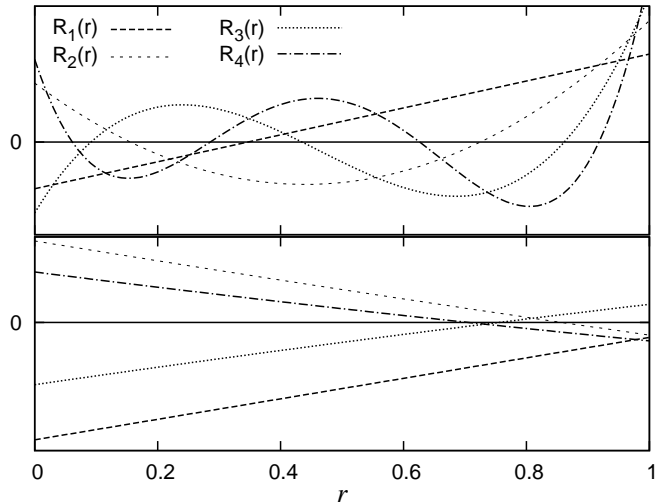


Figure 1. Orthonormal polynomials of degrees 1, 2, 3, and 4 with respect to $w(r) = \exp[-7.67(r/0.5)^{1/4}]$. Orthonormality holds in $0 < r < 1$ (upper panel) and $0 < r < \infty$ (lower panel). The functions in the lower panel are hardly distinguishable, hence lack linear independence. This is due to large variation in the polynomials coefficients, so the high order details are not visible. The functions in the top panel are distinguishably different.

2.4 Integration limits

When generating the radial polynomials (Section 2.3), a sensible integration limit must be chosen. In Shapelets one can integrate r from 0 to ∞ thanks to the Gaussian function’s localized profile. For Sérsic functions in general, however, the profile may not be localized enough to allow for an infinitely large domain. This is generally true for any galaxy and stellar profile used as a weight function.

The problem with using an infinitely large domain is the lack of mutual independence among the fitting functions. In order to construct a model as a linear combination of fitting functions, each fitting function must be distinct so that there is no redundancy in their shapes. Figure 1 shows the polynomials that are generated using a weight function (Equation 7) with $\lambda = 4$. We find that limiting the orthogonality to a finite domain preserves linear independency better than extending to an infinitely large domain.

We conveniently choose $0 < r < 1$ for our domain. For a square image stamp of $2N \times 2N$ pixels, r would be normalized to have units of $1/N$ pixels. It also allows us to constrain $0 < k < 1$, as the scale radius is always positive, and a galaxy should be well captured in a stamp.

2.5 Completeness

Although the fitting functions of Sersiclets are indeed mutually orthonormal, they are not necessarily complete. As a result, Equation 5 does not necessarily converge, even at high n_{\max} . The basis functions in both Cartesian and Polar Shapelets are complete, meaning that Equation 5 can converge for any arbitrary $f(r, \phi)$ as $n_{\max} \rightarrow \infty$.

The incompleteness of Sersiclets is shown in Figure 2. It shows the average difference squared per pixel $\langle \Delta \text{pix}^2 \rangle$ when decomposing a noiseless elliptical object on a 128×128 grid by integrating Equation 5 with χ_{mn}^* , and exploiting or-

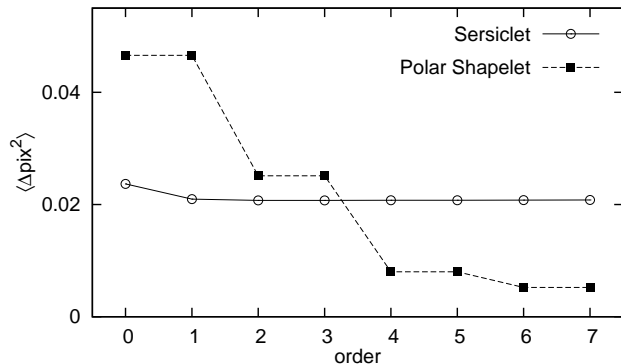


Figure 2. Convergence of Equation 5, represented by the average difference squared per pixel $\langle \Delta \text{pix}^2 \rangle$ when decomposing a high resolution and noiseless elliptical profile. Polar Shapelets are clearly more efficient at describing arbitrary profiles.

thonormality to obtain each A_{mn} . The reconstruction using Sersiclets does not improve even as the order increases; in fact, the reconstruction becomes slightly worse because higher order contributions are as small as the discretization error. Clearly, Sersiclets fail to decompose even a simple elliptical object.

For this reason, we would not attempt the decomposition by including higher order fitting functions. In the next section we take a different approach – throwing away all circularly asymmetric components. The lack of contribution by those components is an important rationale of our technique to reduce the set of fitting functions.

2.6 Fitting set reduction

It is clear from Section 2.5 that the fitting set should be reduced in order to take advantage of the matched filter due to the lack of completeness. In the following we reduce our set of fitting functions to only the circularly symmetric components ($m = 0$), and we introduce ellipticities by transforming the now perfectly circular model by “scaling” and “rotating”, which yield unique values of e_1 and e_2 . This is similar to the process described in Bernstein & Jarvis (2002).

The set of “reduced Sersiclets” has two advantages; eliminating the $m \neq 0$ components not only cures the overfitting problem, but it also offers a dramatic increase in speed as the number of terms in Equation 5 now increases like $O(n_{\max})$ rather than $O(n_{\max}^2)$. It also provides a direct estimate of e_1 and e_2 , which are treated as asymmetric scaling parameters for the fitting function.

We focus on fitting profiles that are smooth, centrally peaked, and elliptical in general. These fitting functions are not suitable for studying galaxy morphology, as they cannot provide information about a galaxy’s detailed structure. In weak gravitational lensing studies, however, the details in the typical faint images analyzed are dominated by noise and should not be fitted. Therefore our reduced fitting set offers a natural regularization process which is missing in the standard Shapelet approach. Our method is a hybrid of Shapelets and fitting techniques, where we do allow some decomposition into fitting functions, but those fitting functions are by construction axisymmetric and therefore pre-

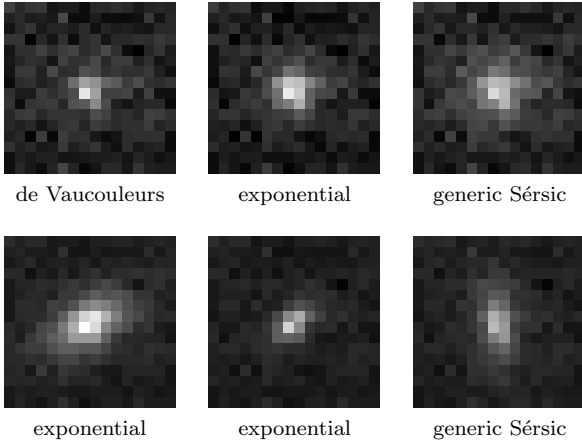


Figure 3. A subset of noisy images for our experiment. Top: Circular profiles to test the full fitting set. Bottom: Elliptical profiles to test the reduced fitting set. De Vaucouleurs and exponential profiles have $\lambda = 4$ and $\lambda = 1$, respectively.

vent isophote mixing (i.e. overfitting) as higher order fitting techniques do.

3 EXPERIMENT

Our experiment at this stage is not a rigorous test for shape measurement, as our test cases (Figure 3) are idealized profiles without PSF convolution. Rather, we are exploring the effect of using a variety of weight functions with different (k, λ) . Our test cases consist of both circular and elliptical profiles. We generated two-dimensional reduced χ^2 maps of k vs order at fixed λ values.

The χ^2_{red} maps are then compared against those generated using Polar Shapelets, which we will refer to simply as “Shapelets” in the following discussion. In Shapelets’ case, the r coordinate is also normalized to $0 < r < 1$. The “scaling-factor” β in Shapelets is now comparable to k in Sersiclets, which is relative to the size of the image. The model fits for both Sersiclets and Shapelets were computed using HROTHGAR³ implemented in C.

3.1 Results – Circular models using the full fitting set

We first test the full fitting set by fitting against circular profiles. In Figure 4, we see that convergence of $\chi^2_{\text{red}} \approx 1$ is achieved very quickly. This is not surprising as the weight functions in the models are indeed realistic. More importantly, we find that the fits are insensitive to the choice of (k, λ) after the first few orders. This robustness allows us to obtain good fits without searching for an optimal (k, λ) . This result is useful in fitting large collections of objects, where families of objects can simply share the same pair of (k, λ) without compromise.

Comparing the χ^2_{red} maps and image reconstructions

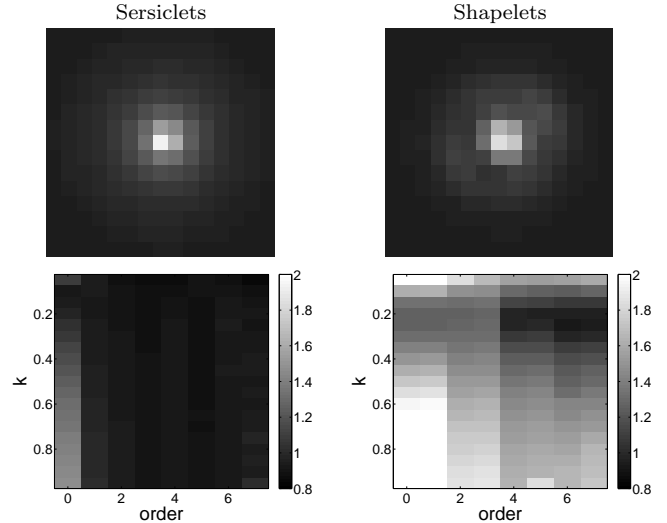


Figure 4. Model fits to the de Vaucouleurs ($1/\lambda = 0.25$) profile using the full fitting set. Upper panels: Sersiclets (order 1, $1/\lambda = 0.3, k = 0.3$) (left) and Shapelets (order 4, $k = \beta = 0.2$) (right). χ^2_{red} values are 0.9371 and 0.9737, respectively. Lower panels: χ^2_{red} maps of the same fits as the upper panels.

between Sersiclets and Shapelets reveals Sersiclets’ advantage. In very non-Gaussian cases such as the de Vaucouleurs case, Sersiclets converge at a much lower order than Shapelets. In fact, Shapelets require low signal-to-noise ratios in order to render an illusion of “good fit”. From Figure 4, we see that Shapelets’ lowest order best fit at order = 4 already shows signs of noise fitting; the model is not smooth, and it shows non-circular isophotes. Sersiclets, though, can recover the smooth and circular profile at orders 0 or 1.

3.2 Results – Elliptical model using the reduced fitting set

For the elliptical profiles, the χ^2_{red} maps (Figure 5) are very similar to those shown in Figure 4. This means that the $m \neq 0$ components were indeed not important, and Sersiclets’ robustness in (k, λ) are preserved. Fitting set reduction as described in Section 2.6 has been done to both Sersiclets and Shapelets. In Shapelets’ case, since $m = 0$ components do not exist for odd orders, only even orders were possible. As seen in the image reconstruction in Figure 5, the Shapelet fit no longer shows noise fitting thanks to fitting set reduction.

The residuals of measured e_1 values corresponding to each input value have been plotted in Figure 6. It is clear that as the fit improves with higher orders, the scatter in the measured ellipticity is reduced. For Shapelets, the solution does not show robustness in k as the measured ellipticities are more scattered than the Sersiclets’ case.

3.3 Discussion

Sersiclets’ robustness in (k, λ) and its ability to converge in relatively low orders comes from the abundance of its degrees of freedom in the model. For the full fitting set, Equation 5 has $(n_{\text{max}} + 1)^2$ terms in the summation as the angular quantum number m increases in steps of 1. Polar Shapelets, however, have only $(n_{\text{max}} + 1)(n_{\text{max}} + 2)/2$ terms

³ <http://hrothgar.sourceforge.net/>

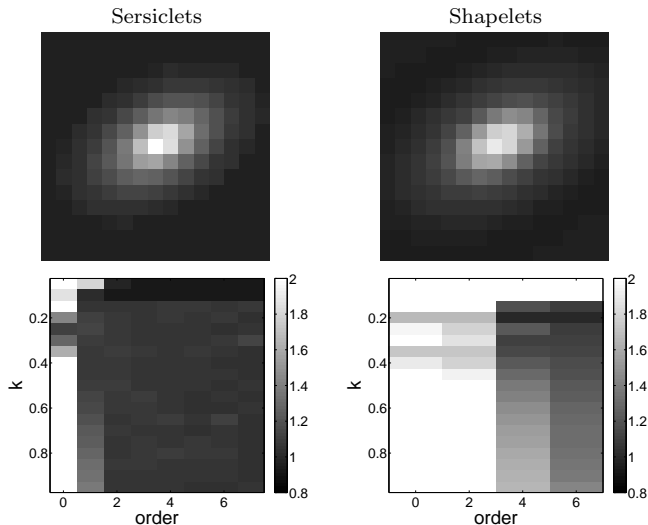


Figure 5. Model fits to the elliptical exponential ($1/\lambda = 1$) profile using the reduced fitting set. Upper panels: Sersiclets (order 4, $1/\lambda = 0.8$, $k = 0.2$) (left) and Shapelets (order 4, $k = \beta = 0.2$) (right). χ_{red}^2 values are 1.0000 and 1.0634, respectively. Lower panels: χ_{red}^2 maps of the same fits as the upper panels.

Table 1. Input parameters for the elliptical models in Figure 6. Each model is 16×16 pixels in dimension, and has peak $S/N \approx 25$.

e_1	e_2	k	$1/\lambda$
0.130	0.225	0.43	1.0
0.244	0.089	0.43	1.0
0.180	0.186	0.43	1.0
-0.263	0.164	0.24	1.0
0.274	0.146	0.24	1.0
0.011	0.310	0.24	1.0
0.012	0.069	0.29	0.75
0.066	0.024	0.29	0.75
-0.066	0.024	0.29	0.75
-0.140	0.348	0.28	0.75
0.116	0.357	0.28	0.75
-0.367	-0.078	0.28	0.75

as m increases in steps of 2 at a given order of n . For the reduced fitting set, Sersiclets have $n_{\text{max}} + 1$ terms, and Polar Shapelets have only $n_{\text{max}}/2 + 1$ terms. Together with λ and k , Sersiclets would have about twice as many degrees of freedom as Polar Shapelets. To facilitate a fair comparison, Figure 6 compares Sersiclets at order 3 against Shapelets at order 6 in the second and third panels. This ensures that the test uses the same degrees of polynomials available to each decomposition technique.

A drawback of Sersiclets is numerical instability. Hermite or associated Laguerre polynomials in Shapelets can be generated very easily with elementary operations, whereas the general Sersiclet polynomials require gamma functions. In particular, the analytical solution to the integral

$$\int_0^1 r^j \exp[-b_\lambda (r/k)^{1/\lambda}] dr \quad (j = 1, 2, \dots) \quad (8)$$

which is ubiquitous in Section 2.3, can be written as

$$\lambda (b_\lambda k^{-1/\lambda})^{-\lambda - j\lambda} \left[\Gamma(\lambda + j\lambda) - \Gamma(\lambda + j\lambda, b_\lambda k^{-1/\lambda}) \right] \quad (9)$$

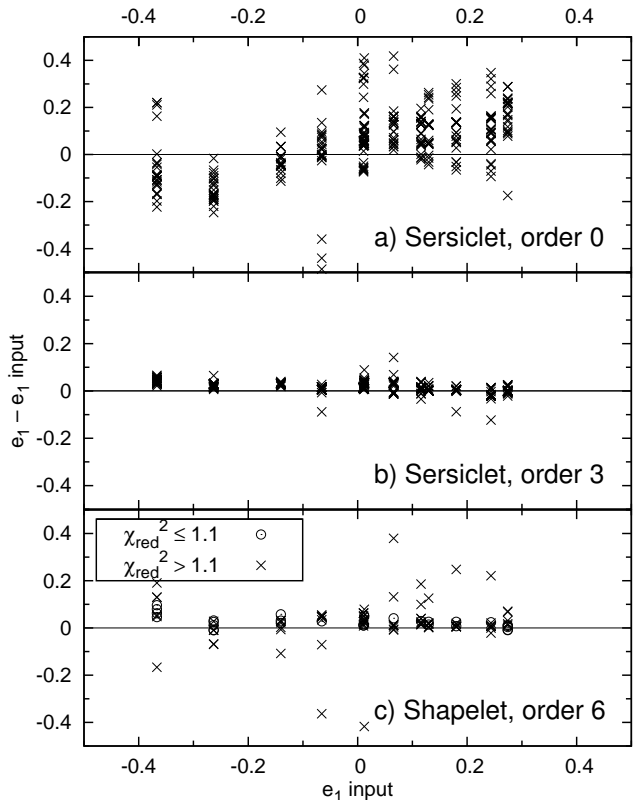


Figure 6. e_1 residuals measured using the reduced fitting set. Each column of points is an object (Table 1), and each data point is a different (k, λ) , where $0.05 \leq k \leq 0.95$ in steps of 0.1 and $0.4 \leq 1/\lambda \leq 1.0$ in steps of 0.2 (for Sersiclets). The behavior of the best fit e_2 is very similar to those in e_1 . At order 3, Sersiclets can achieve $\chi_{\text{red}}^2 \approx 1$ and measure e with only a small dispersion. In contrast, Shapelets can do so only at a certain range of k (or β) that produces good fits (See Figure 5). At a given “order”, Sersiclets have about twice as many degrees of freedom as Shapelets.

where $\Gamma(z)$ and $\Gamma(a, z)$ are the complete and incomplete gamma functions, respectively, and $b_\lambda = 2\lambda - 1/3$ as before. At first glance, it may be tempting to use the analytical solution because it exists and gamma functions can be readily evaluated. Upon closer inspection, though, Equation 9 evaluates the difference between two gamma functions, each on the order of $(\lambda + j\lambda)!$. The difference is then scaled by a number raised to the power of $-(\lambda + j\lambda)$. One needs to be careful when evaluating such an expression if $(\lambda + j\lambda)!$ becomes large, especially when using numerical libraries with single precision. Alternatively, the integrand in Equation 8 is a smooth function, so the integral can be evaluated directly without implementing the analytical solution.

Sersiclets can be generalized to different weight functions. In our derivation, although we have chosen the Sérsic function as our weight function, the process would still be the same for any weight functions which are intrinsically elliptical without explicit angular dependence. This allows for modeling different types of objects such as the PSF using the Moffat profile as the weight function. The integration limit of the radial component, as we discussed in Section 2.4, can be either finite or infinite depending on whether the weight function is sufficiently localized.

4 CONCLUSION

We presented an extension of Shapelets by using an arbitrary weight function in place of the Gaussian function. As galaxies' light profiles follow the Sérsic profile on average, we used the Sérsic function as our weight function. This allowed us to fit cuspy galaxies at lower orders than Shapelets could.

Because the Sérsic function lacks analytical properties, we used the Gram-Schmidt process to generate the orthonormal polynomials as radial components for the fitting functions, where the integrals in the process must be evaluated numerically. As the Sérsic profile has poor local support, the integration limit must be truncated to a finite limit.

We found that the full set of fitting functions for Sersiclets cannot decompose an arbitrary image even at high orders, as the fitting functions do not form a complete set. Instead of modeling objects using all fitting functions, we reduced the fitting set to only the circularly symmetric components ($m = 0$). The model was then sheared by e_1 and e_2 to render elliptical shapes. The reduced set of fitting functions defines a hybrid method which combines the most interesting features of the basis decomposition and the fitting technique.

Our experiments so far only focused on idealized images simulated using known profiles and noise. Both the full and the reduced Sersiclets outperformed Shapelets, as we expected. The Shapelet matched filter's true performance will be tested in a future paper on image simulations such as those for GREAT08 (Bridle et al. 2008). The C code to evaluate Sersiclet models is publicly available on request.

ACKNOWLEDGMENTS

We are grateful to Ariel Zhitnitsky for inspiring discussions at the beginning of this work, and Peter Melchior for valuable comments. We also thank the anonymous referee for detailed and very constructive comments on the manuscript. Wayne Ngan, LVW, and Henk Hoekstra are supported by NSERC and CIFAR.

REFERENCES

- Bergé, J., Pacaud, F., et al., 2008, MNRAS, 385, 695.
 Bernstein, G., Jarvis, M., 2002, AJ, 123, 583.
 Bridle, S., et al., 2008, arXiv:0802.1214.
 Heymans, C., Van Waerbeke, L., et al., 2006, MNRAS, 368, 1323.
 Hoekstra, H., Jain, B., 2008, arXiv:0805.0139.
 Kitching, T., Miller, L., et al. 2008, arXiv:0802.1528.
 Kuijken, K., 2006, A& A, 456, 827.
 Massey, R., Heymans, C., et al., 2007, MNRAS, 376, 13.
 Massey, R., Refregier, A., 2005, MNRAS, 359, 1277.
 Miller, L., Kitching, T., et al., 2007, MNRAS 382, 315.
 Munshi, D., Valageas, P., et al., 2008, PhR, 462, 67.
 Peng, C., Ho, L., et al., AJ, 2002, 124, 266.
 Refregier, A., 2003, MNRAS, 338, 35.
 Refregier, A., Bacon, D., 2003, MNRAS, 338, 48.
 Sérsic J. L., 1968, Atlas de Galaxias Australes (Córdoba: Obs. Astron., Univ. Nac. Córdoba).

This paper has been typeset from a $\text{\TeX}/\text{\LaTeX}$ file prepared by the author.